Proc. Natl. Sci. Counc. ROC(A)
Vol. 24, No. 4, 2000. pp. 310-315

Aligning Mechanism of an *In Situ* Poled Nonlinear Optical Polymer Prepared Using the Chemical Vapor Deposition Method

PAO-KENG YANG*, JUNG-YAW HUANG*,†, AND JWO-HUEI JOU**

**Institute of Electro-Optical Engineering*
Chiao Tung University
Hsinchu, Taiwan, R.O.C.
***Department of Materials Science and Engineering*
Tsinghua University
Hsinchu, Taiwan, R.O.C.

(Received October 18, 1999; Accepted December 15, 1999)

ABSTRACT

Second harmonic (SH) microscopy was applied to investigate an in-plane electric-field poled polymer. We show that the local orientation of the nonlinear optical (NLO) chromophore can be deduced from two SH images obtained with different polarization combinations. A model was developed to illustrate the aligning dynamics of NLO chromophores during the film deposition process.

Key Words: nonlinear optical polymer, second harmonic microscopy, aligning dynamics

I. Introduction

Two major advances have been made in the development of organic nonlinear optical (NLO) polymers. The first focused on the synthesis of suitable chromophores with large NLO responses. The second advance aimed to arrange these NLO chromophores in polar ordered structures. Crystal growth and various poling techniques were employed to create such structures. Unfortunately, to minimize the free energy crystal growth normally tends to arrange polar molecules in pairs with their dipole moments antiparallel to each other. Therefore, the second-order NLO responses are averaged out at macroscopic scales. To avoid such centro-symmetric arrangements, an electric poling technique has been developed to provide a simple while efficient method for creating a polar ordering structure. However, to yield a large effective optical nonlinearity, a vertically poled NLO polymer (Huang *et al*., 1995; Liao *et al*., 1995) must be oriented so that the surface normal will be tilted by a large angle from the light propagating direction. This causes inconvenience in practical applications. In-plane poling geometry can offer better tensor properties that lead to more effective second-order nonlinearity.

Recently, a novel chemical vapor deposition technique (Nagamori *et al*., 1992; Jou *et al*., 1997) has been developed. With this preparation procedure, NLO chromophores are deposited simultaneously with monomers onto a glass substrate. By applying an electric field to a pair of in-plane electrodes, an *in situ* poling can also be employed (Wu *et al*., 1997). However, it is still unclear how the NLO chromophores are oriented during the film deposition process.

Second-harmonic generation (SHG) is known to be a fast, quantitative technique for probing materials with polar structures. This method is based on the generation of second harmonic (SH) light from a polar material or surfaces and interfaces where the inversion symmetry is broken. In a typical SHG measurement, a sample is illuminated with a high peak-power laser beam. The generated SHG signal is detected and then integrated over the whole laser beam and pulse duration. The signal carries information about the material's properties averaged over the illuminated area. To probe the local structure of a material, SH microscopy (Schultz and Seebauer 1992; Flörsheimer *et al*., 1994, 1996, 1997a, 1997b; Uesu *et al*., 1995; Kurimura and Uesu., 1997; Smilowitz *et al*., 1997; Bozhevolnyi *et al*., 1998; Vydra and Eich., 1998; Cernusca *et al*., 1998) can be used to spatially resolve optical nonlinearity. The spatial distribution of NLO susceptibili-

†To whom all correspondence should be addressed.

ty can be used to deduce the local symmetry and ordering of the material being studied.

In this paper, we shall present a model of the aligning dynamics in a chemical vapor deposited NLO polymer film poled with an in-plane electrode. The theory is then applied to analyze the SH microscopic results of the film.

II. Experimental Setup

1. Second Harmonic Microscopy

To generate sufficient SH photons for imaging purposes, we used a Q-switched Nd:YAG pulsed laser with a repetition rate of 10 Hz. The experimental setup for the second harmonic microscope is shown in Fig. 1. A lens with a focal length of 50 cm focused the fundamental beam at 1.064 μm. The focused spot size on the sample was about 130 μm. The average power was kept at 15 mW, which corresponded to a peak power of 280 MW/cm^2. The second harmonic signal at 532 nm was separated from the fundamental by using a series of filters to protect the microscope optics and obtain a high signal-to-noise ratio. After passing through a projection lens, the second harmonic signal was detected with a backside-illuminated charge-coupled device (CCD) camera. The CCD had a quantum efficiency of more than 80% from 500 nm to 800 nm.

2. Sample Preparation

The samples were prepared using a chemical vapor deposition (CVD) process, which simultaneously deposits NLO chromophore and two monomers onto a glass substrate. An electrode array with 0.1 mm separation had been fabricated on glass substrates. The co-evaporation was performed using 0.4 gram of disperse red 1 (DR-1) chromophores kept at 80ºC–140ºC with one monomer 6F-dianhydride (6FDA) at 85ºC–110ºC and the other 4,4'-oxydianiline (ODA) at 70ºC–90ºC. The deposition apparatus is depicted in Fig. 2. The NLO chromophores were polar oriented during the film deposition process by applying a voltage of 1.5 kV on the electrodes, which yielded a dc field strength of about 0.15 MV/cm in the electrode gap. Typical film thickness was measured and found to be 500 Å.

3. Second Harmonic Microscopic Study of a Poled Polymer Film

In Fig. 3(a), a second harmonic microscopic image obtained on in-plane poled NLO film with the incident beam polarized perpendicular to the dc poling field is presented. The corresponding SH image with the incident beam polarized parallel to the dc poling field is shown in Fig. 3(b). For both measurements, an analyzer was employed to select the SH polarization component which was parallel to the dc poling field. The second harmonic intensity shown in Fig. 3(b) is about three times stronger than that shown in Fig. 3(a).

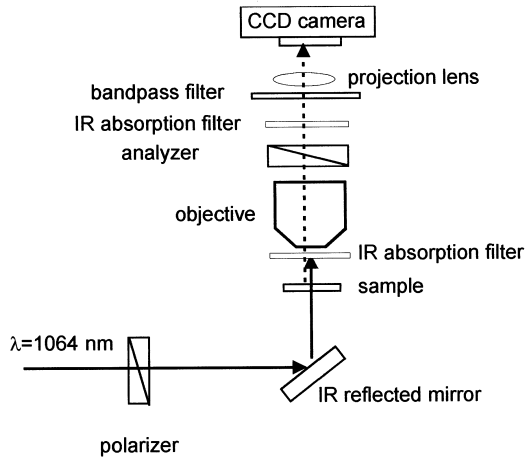

Fig. 1. Schematic diagram of a second harmonic microscope.

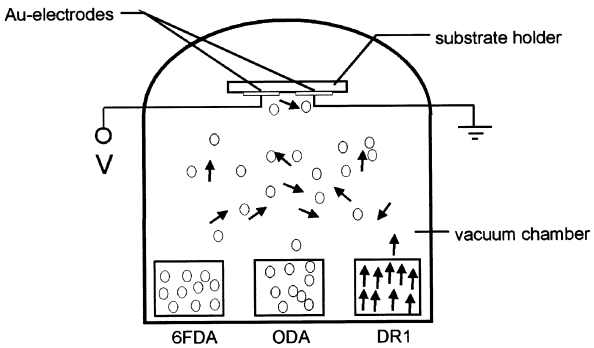

Fig. 2. Schematic diagram of a vapor deposition polymerization apparatus with an *in situ* poling setup.

III. Theory

1. Relation between the Second-Harmonic Intensity and the Orientation of the NLO Chromophore

Assuming that the NLO chromophores used are rod-like in shape, the NLO susceptibility of a poled polymer can then be related to the molecular hyperpolarizability of the NLO chromophores by

$$\chi_{zxx}^{(2)}(-2\omega;\omega,\omega)$$

$$= NL_{zz}(2\omega)L_{xx}{}^2(\omega)\alpha_{\xi\xi\xi}^{(2)}(-2\omega;\omega,\omega)$$

$$< \cos^2\phi\cdot\cos\theta\cdot\sin^2\theta >, \qquad \textbf{(1)}$$

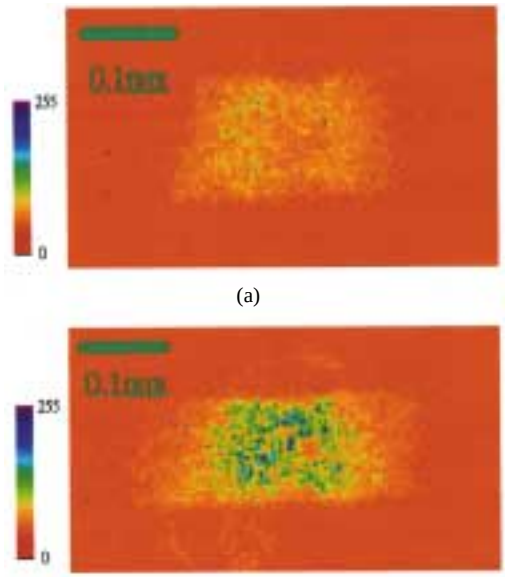

Fig. 3. Second harmonic images of an in-plane electric-field-poled polymer film. The polarization of the incident fundamental beam is (a) perpendicular, (b) parallel to the dc poling field. The SH polarization is parallel to the dc poling field in both images.

$$\chi_{zzz}^{(2)}(-2\omega;\omega,\omega)$$

$$= NL_{zz}(2\omega)L_{zz}^{\ 2}(\omega)\alpha_{\xi\xi\xi}^{(2)}(-2\omega;\omega,\omega)<\cos^3\theta>, \quad \textbf{(2)}$$

where N is the number density of the chromophores; $\alpha_{\xi\xi\xi}^{(2)}$ denotes the dominant component of the rod-like chromophore; $L_{ii}(\omega)$ is the local-field correction factor at a frequency ω with polarization along i; and < > represents an average over the orientational distribution of the NLO chromophores:

$$\langle g(\Omega)\rangle = \int g(\Omega) f(\Omega) d\Omega. \quad \textbf{(3)}$$

Here, $f(\Omega)d\Omega$ denotes the probability that the chromophores are oriented in the solid-angle interval of Ω to $\Omega + d\Omega$. The relations among the different coordinates systems are shown in Fig. 4. From the SHG intensities shown in Fig. 3(a) and (b), we have

$$\frac{I(2\omega)_{z\leftarrow xx}}{I(2\omega)_{z\leftarrow zz}} = \left|\frac{\chi_{xyy}^{(2)}}{\chi_{xxx}^{(2)}}\right|^2 \cong \frac{<\cos^2\phi\cdot\cos\theta\cdot\sin^3\theta>}{<\cos^3\theta>}. \quad \textbf{(4)}$$

The most attractive feature found in Eq. (4) is that the inhomogeneity of the molecular density and local field strength has been removed. The local SH intensity ratio, therefore, directly reflects the local orientational information $f(\Omega)$.

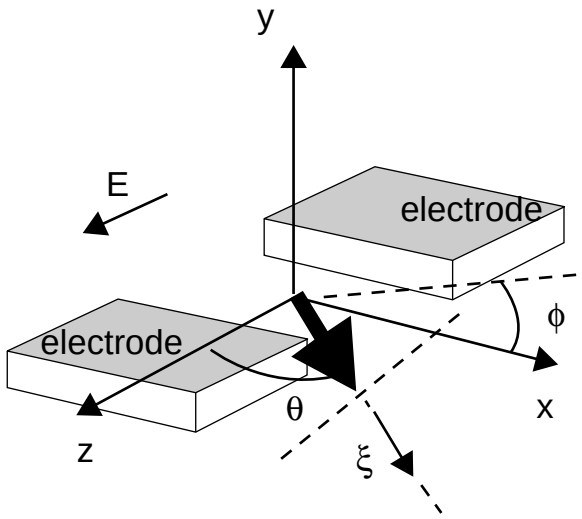

Fig. 4. Schematic diagram showing the relation between different coordinate systems, (x, y, z) and (r, θ, ϕ), and the molecular chain axis ζ for the theoretical model of a poled olymer.

2. A Model of the Aligning Dynamics of the NLO Chromophore during Film Deposition

When DR-1 molecules are thermally evaporated from a heated reservoir, their dipole moments are randomly oriented. As the NLO chromophores approach the substrate, they are influenced by the dc poling field. Assuming that the DR-1 molecules have a dipole moment μ, mass m, and molecular length $2a$, the moment of inertia of the molecule can then be calculated as $I = (1/3)ma^3$ with a rodlike geometry shape.

The equation of motion for a polar molecule in a uniform poling field is described by

$$I\frac{d^2\theta}{dt^2} = \vec{\mu}\times\vec{E} = -\mu E\sin\theta. \quad \textbf{(5)}$$

For small-angle deviation, we can linearize the equation by using $\sin\theta \cong \theta$. Therefore, Eq. (5) essentially depicts a precession motion with a period of

$$t_p = 2\pi\sqrt{\frac{I}{\mu E}}. \quad \textbf{(6)}$$

The dipole moment precesses along the applied dc poling field in a way similar to that of the magnetic dipole moment in a magnetic field (Fig. 5). We shall characterize the dynamical process with three time scales in order to yield a clearer picture of the deposition process.

The first time scale represents the period of oscillation described by Eq. (6). We should note that the higher

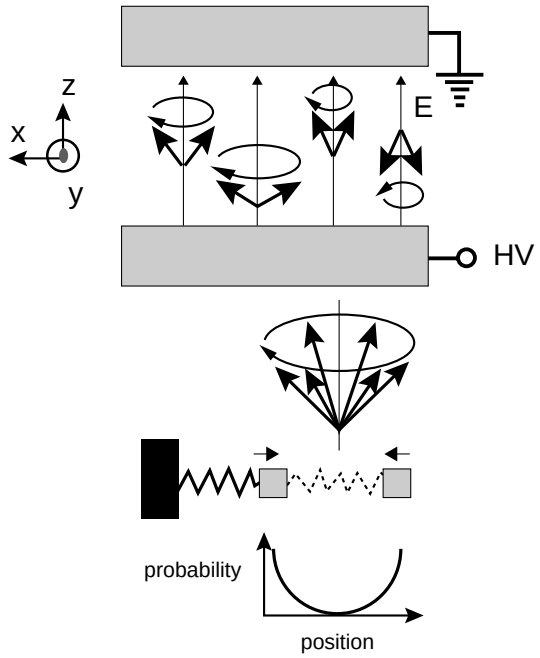

Fig. 5. Dipole precession in a dc poling field and the corresponding probability distribution.

order terms in Eq. (5) from the expansion of $\sin\theta$ only change the oscillating period slightly (Marion, 1970). Therefore, Eq. (6) is still useful for estimating the magnitude of the precession period. In the present case, the DR-1 chromophore had a molecular mass of 314 g/mol, a dipole moment of 8.72 D (D: Debye, 1D = 3.336×10^{-30} C.m), and $2a$ = 14.5 Å. The period of oscillation was then calculated and found to be ~10^{-10} sec.

The second time scale is the traveling time of DR-1 through the poling zone. The length of the poling zone is estimated to be 0.3 μm from the electrode thickness. Therefore, it takes DR-1 molecules 1.7×10^{-9} s to arrive at the substrate.

The third time scale is the collision time of DR-1 molecules in a vacuum chamber. The typical mean free time at room temperature under standard atmospheric pressure is about 10^{-10} s (Sears and Salinger, 1975). In our experiment, the deposition process began with a pressure of 5×10^{-5} mbar. Owing to the low density of molecules in our vacuum chamber, the mean free time increased to about 3×10^{-8} s. This time was much longer than the traveling time. Therefore, DR-1 molecules could be assumed to pass through the poling zone without colliding with other molecules.

Note that a damping process is needed to damp the vibrating dipole moments, which allows the dipole direction to point to the poling electric field. Since DR-1 molecules do not collide with each other in the poling region, this damping effect will not occur. When the precession period is longer than the traveling time, the dipole direction on the substrate surface is very close to the pointing direction as DR-1 molecules enter the poling zone. The resulting orientation distribution should, therefore, be isotropic as shown in Fig. 6(a). In our experiment, the precession period was much shorter than the traveling time, so the dipole moment of a DR-1 could precess many times during its trip through the poling zone.

Recent studies (Hasegawa *et al*., 1996) on polyimides have revealed a chain orientation in the film plane. Following the definition given for coordinates, we assume that DR-1 molecules on a substrate have a long molecular axis lying on the plane of the substrate (*i.e*. the x-z plane). The precessing dipole projected onto the x-z plane essentially behaves like a simple harmonic motion. From either classical mechanics or quantum mechanics, we know that an oscillator can be found with high probability at two extreme positions where the velocity is zero. The precession motion, therefore, causes the dipole orientation to point to the two orientation extremes. The number of molecules lying between θ and $\theta + d\theta$ is weighed with $\sin\theta$. The resulting orientational distribution is depicted in Fig. 6(b). Note that the distribution is still nonpolar and will not exhibit any SH signal (*i.e*., the dc poling field which causes the dipole moment to precess can not generate a polar structure before DR-1 anchors on the substrate). Thus, we conclude that the main aligning process should take place after DR-1 molecules are deposited on the substrate.

If no dc electric field is applied, the DR-1 molecules are deposited on the substrate isotropically. When the in-plane dc electric field is applied, the molecules then experience interaction with orientation-dependent potential energy. The resulting orientation distribution is given by

$$f(\Omega) = \frac{\exp[-(U - L(0)\mu \cdot E)/kT]}{\int \exp[-(U - L(0)\mu \cdot E)/kT]d\Omega}, \qquad \textbf{(7)}$$

where U denotes the potential energy created by the elastic interaction with the neighboring polymer matrix or substrate (Kuzyk *et al*., 1990); $L(0)$ accounts for the local field correction for the dc poling field. The thermal perturbation from the finite temperature requires that the molecules have a Boltzman distribution. The orientational distribution can reach thermal equilibrium in a time scale that is determined by the rotational diffusion of the chromophores and the viscosity of the polymeric matrix at the poling temperature. By expanding $\cos\theta = \mu \cdot E / |\mu \cdot E| \cong 1 - (1/2)\theta^2$ around the equilibrium orientation, the distribution function in Eq. (7) can then be approximated by a Gaussian distribution $\exp[-((\theta - \theta_0)/\Delta\theta)^2]$, where $\Delta\theta$ denotes the angular spread; θ_0 is the average polar angle. Here, θ_0 is not zero owing to a combined effect of the precession and field-induced alignment. The orientational dis-

tribution is presented in Fig. 6(c). Using Eq. (7), the SH intensity ratio can then be rewritten as

$$\frac{I(2\omega)_{z\leftarrow xx}}{I(2\omega)_{z\leftarrow zz}} = \left| \frac{\int_0^{\pi} \exp[-(\frac{\theta-\theta_0}{\Delta\theta})^2]\sin^2(\theta)\cos(\theta)\sin(\theta)d\theta}{\int_0^{\pi} \exp[-(\frac{\theta-\theta_0}{\Delta\theta})^2]\cos^3(\theta)\sin(\theta)d\theta} \right|^2 . \quad \textbf{(8)}$$

After the poling field is switched off, the orientational distribution starts to "diffuse," which causes the SH intensity to decrease accordingly. Our SH images were obtained as soon as the film was prepared. The angular spread $\Delta\theta$ could be assumed to be small. By using a δ-function for the azimuthal distribution of the NLO chromophores, Eq. (8) yielded an average angle:

$$\theta_0 = \tan^{-1}\left[\sqrt[4]{\frac{I(2\omega)_{z\leftarrow xx}}{I(2\omega)_{z\leftarrow zz}}}\right]. \quad \textbf{(9)}$$

The nonzero angular width in the polar distribution led to a minor deviation from that predicted by Eq. (9). However owing to the simplicity, we still employed Eq. (9) to determine the local orientation variation of the NLO chromophore from the measured SH images shown in Fig. 3. The result is presented in Fig. 7. Due to the existence of mirror symmetry relative to the y-z plane, only the left portion of the orientation variation is shown in a vector field format.

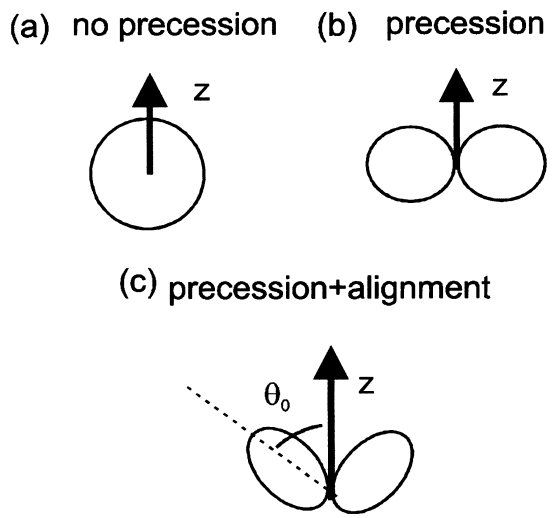

Fig. 6. Orientational distributions originating from different dynamic processes: (a) isotropic when the precession period is much longer than the traveling time; (b) a precession-induced unpolar distribution when the traveling time is much longer than the precession period; (c) poling-field-induced polar distribution.

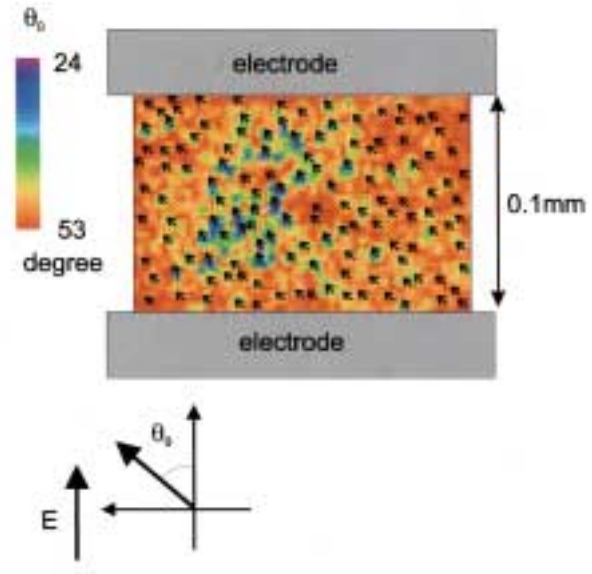

Fig. 7. Vector diagram of the local orientation of NLO chromophores. The orientational distribution is assumed to be symmetric about the y-z plane. Only the left portion is shown in the figure.

IV. Conclusion

The observed second-harmonic intensity variation within the illuminated area indicates that the NLO chromophores were not uniformly oriented during the deposition process. The film defects, which were clearly observed with an SH microscope, seriously degraded the NLO response of the films. With further improvement in the preparation procedure, this type of NLO polymeric film can be used to realize micrometer-scales NLO devices. In this regard, second-harmonic microscopy serves as an ideal tool for spatially resolved study of this new NLO material.

In summary, we have applied second harmonic microscopy to characterize an NLO polymer poled with in-plane electrodes. From the recorded second harmonic intensity patterns, we have successfully obtained information about the local orientation of the nonlinear optical chromophores in the polymer matrix.

References

Bozhevolnyi, S. I., J. M. Hvam, K. Pedersen, F. Laurell, H. Karlsson, T. Skettrup, and M. Belmonte (1998) Second harmonic imaging of ferroelectric domain walls. *Appl. Phys. Lett*., **73**, 1814-1816.

Cernusca, M., M. Hofer, and G. A. Reider (1998) Coherence effects in second harmonic interface imaging. *J. Opt. Soc. Am*., **B15**, 2476-2480.

Flörsheimer, M., H. Looser, M. Küpfer, and P. Günter (1994) *In situ* im-

aging of Langmuir monolayers by second-harmonic microscopy. *Thin Solid Films*, **244**, 1001-1006.

Flörsheimer, M., C. Radüge, H. Salmen, M. Bösch, R. Terbrack, and H. Fuchs (1996) In-situ imaging of Langmuir monolayers by second-harmonic microscopy. *Thin Sold Films*, **284-285**, 659-662.

Flörsheimer, M., H. Salmen, M. Bösch, C. Brillert, M. Wierschem, and H. Fuchs (1997a) Molecular surface orientation field of a Langmuir monolayer determined by second-harmonic microscopy. *Adv. Mater*., **9**, 1056-1060.

Flörsheimer, M., H. Salmen, M. Bösch, C. Brillert, M. Wierschem, and H. Fuchs (1997b) Second-harmonic microscopy — a quantitative probe for molecular surface order. *Adv. Mater*., **9**, 1061-1065.

Hasegawa, M., T. Matano, Y. Shindo, and T. Sugimura (1996) Spontaneous molecular orientation of polyimides induced by thermal imidization. 2. In-plane orientation. *Macromolecules*, **29**, 7897-7909.

Huang, J. Y., C. L. Liao, W. T. Whang, and C. J. Chang (1995) Thermal stability of second-order nonlinearty in poled polymeric films. *Jpn. J. Appl. Phys*., **34**, 136-144.

Jou, J. H., H. S. Wu, J. F. Chiou, P. K. Yang, and J. Y. Huang (1997) A real-time poling approach for preparing second-order nonlinear optical polymer thin film. *Thin Solid Films*, **304**, 299-302.

Kurimura, S. and Y. Uesu (1997) Application of second harmonic generation microscope to nondestructive observation of periodically poled ferroelectric domains in quasi-phase-matched wavelength converters. *J. Appl. Phys*., **81**, 369-375.

Kuzyk, M. G., R. C. Moore, and L. A. King (1990) Second-harmonic-generation measurements of the elastic constant of a molecule in a polymer matrix. *J. Opt. Soc. Am*., **B7**, 64-72.

Liao, C. L., J. Y. Huang, C. J. Chang, and W. T. Whang (1995) Nonlinear optical properties and poling dynamics of a side-chain polymeric film. *Nonlinear Optics*, **12**, 309-326.

Marion, J. B. (1970) *Classical Dynamics of Particles and System*, 2nd Ed., Chap. 5. Academic Press, New York, NY, U.S.A.

Nagamori, H., K. Kajikawa, H. Takezoe, A. Fukuda, S. Ukishima, M. Iijima, Y. Takahashi, and E. Fukada (1992) Poling dynamics and negligible relaxation in aromatic polyurea study by *in situ* observation of second-harmonic generation. *Jpn. J. Appl. Phys. Part* 2, **31**, L553-L555.

Schultz, K. A. and E. G. Seebauer (1992) Surface diffusion of Sb on Ge(111) monitored quantitatively with optical second harmonic microscopy. *J. Chem. Phys*., **97**, 6958-6967.

Sears, F. W. and G. L. Salinger (1975) *Thermodynamics, Kinetic Theory, and Statistical Thermodynamics*, 3rd Ed., Chap. 10. Addison-Wesley, Reading. MA, U.S.A.

Smilowitz, L., Q. X. Jia, X. Yang, D. Q. Li, D. McBranch, S. J. Buelow, and J. M. Robinson (1997) Imaging nanometer-thick patterned self-assembled monolayers via second-harmonic generation microscopy. *J. Appl. Phys*., **81**, 2051-2054.

Uesu, Y., S. Kurimura, and Y. Yamamoto (1995) Optical second harmonic image of 90º domain structure in $BaTiO_3$ and periodically inverted antiparallel domains in $LiTaO_3$. *Appl. Phys. Lett*., **66**, 2165-2167.

Vydra, J. and M. Eich (1998) Mapping of the lateral polar orientational distribution in second-order nonlinear thin films by scanning second-harmonic microscopy. *Appl. Phys. Lett*., **72**, 275-277.

Wu, H. S., J. H. Jou, and Y. C. Li (1997) Real-time poling vapor co-deposition of dye-doped second-order nonlinear optical polymer thin film. *Macromolecules*, **30**, 4410-4414.

化學氣相沉積和即時極化技術製備之非線性光學高分子薄膜的分子動態排列機制

楊寶賡[*] 黃中垚[*] 周卓輝[**]

[*]國立交通大學光電工程研究所
[**]國立清華大學材料工程學系

摘 要

我們應用光二倍頻顯微技術探討以化學氣相沉積法製成的非線性光學高分子薄膜的發色團指向分佈。利用二種不同的入射基頻光場方向所收集到的二倍頻顯微影像，可得出非線性發色團的局部方向排列分佈。我們也發展出一微觀模型以說明發色團在薄膜製備過程的指向動態變化。